



## Predicting Ocean Waves along the U.S. East Coast During Energetic Winter Storms: sensitivity to Whitecapping parameterizations

5 Mohammad Nabi Allahdadi<sup>1</sup>, Ruoying He<sup>1</sup>, and Vincent S. Neary<sup>2</sup>

<sup>1</sup>North Carolina State University, Department of Marine, Earth, and Atmospheric Sciences, Raleigh, NC27695, USA

<sup>2</sup>Sandia National Laboratories, P.O. Box 5800, Albuquerque, NM 87185 - MS1124, USA

*Correspondence to:* Mohammad Nabi Allahdadi (mallahd@ncsu.edu)

10

**Abstract:** The performance of two methods for quantifying whitecapping dissipation incorporated in the SWAN wave model is evaluated for waves generated along and off the U.S. East Coast under energetic winter storms with a predominantly westerly wind. Parameterizing the whitecapping effect can be done using the Komen-type schemes, which are based on mean spectral parameters, or the saturation-based (SB) approach of van der Westhuysen (2007), which is based on local wave parameters and the saturation level concept of the wave spectrum (we use “Komen” and “Westhuysen” to denote these two approaches). Observations of wave parameters and frequency spectra at four NDBC buoys are used to evaluate simulation results. Model-data comparisons show that when using the default parameters in SWAN, both Komen and Westhuysen methods underestimate wave height. Simulations of mean wave period using the Komen method agree with observations, but those using the Westhuysen method are substantially lower. Examination of source terms shows that the Westhuysen method underestimates the total energy transferred into the wave action equations, especially in the lower frequency bands that contain higher spectral energy. Several causes for this underestimation are identified. The primary reason is the difference between the wave growth conditions along the East Coast during winter storms and the conditions used for the original whitecapping formula calibration. In addition, some deficiencies in simulation results are caused along the coast by the “slanting fetch” effect that adds low-frequency components to the 2-D wave spectra. These components cannot be simulated partly or entirely by available wind input formulations. Further, the effect of boundary layer instability that is not considered in the Komen and Westhuysen whitecapping wind input formulas may cause additional underestimation.

15

20

25

### 1 Introduction

30

Spectral wave models, including Simulating Wave Nearshore (SWAN) (SWAN, 2015), solve the equation for conservation of wave action density in the frequency-direction, spatial, and time domains. This equation considers the time variation of spectral energy over the specified geographic domain by considering the local rate of change and



transport terms as well as source terms. The source term in the wave action density equation is the algebraic sum of several terms as follows:

$$35 \quad S_{tot} = S_{wind} + S_{ds,w} + S_{nl4} + S_{nl3} + S_{ds,b} + S_{ds,br} \quad (1)$$

The terms on the right side of the equation are wave growth by wind, wave decay due to whitecapping, nonlinear transfer of wave energy through four-wave (quadruplet) and three-wave (triad) interactions, bottom friction, and depth-induced wave breaking, respectively. Three-wave interaction (triad) as well as bottom friction and depth-induced wave breaking are specific energy source and sink terms for the shallow to the very shallow coastal water environment, whereas the first three terms actively contribute to wave energy development and spectral evolution in  
40 both open-ocean and coastal environments. Quantifying these source terms has been a challenging task and the focus of active research, especially for the wave decay processes associated with whitecapping.

The Komen-type methods for resolving whitecapping dissipation are of the most popular approaches in coastal modeling applications, and are based on the initial study by Hasselmann (1974), formulated by Komen (1984), and  
45 modified by Janssen et al. (1991). This approach represents dissipation of spectral energy as a function of mean spectral frequency and steepness. It is an appropriate approach for simulation of wave height as a result of generation and growth by local wind, and the default method for resolving whitecapping dissipation in SWAN and other popular spectral models like WAM and Mike21-SW. To achieve higher simulation accuracies for wave height and wave period, calibrations of the model for the whitecapping parameter and the wave period parameter delta are necessary  
50 (Allahdadi et al., 2017; Siadatmousavi et al., 2011 and 2012; Kamranzad et al., 2016; Niroomandi et al., 2018; Allahdadi et al., 2004). However, wave model applications for different regions show that Komen-type methods tend to underestimate both peak and mean wave periods. For the case of pure wind wave growth, this problem is the result of underestimating the spectral energy at low frequencies. In the presence of low-frequency swell waves with lower spectral steepness, this method contributes to higher rates of swell energy dissipation and under-prediction of wave  
55 period (van der Westhuysen et al., 2007).

To address these shortcomings of the Komen-type models, Westhuysen et al. (2007) introduced an alternative whitecapping method based on a modified approach by Alves et al. (2003) using the concept of local saturation of spectra instead of mean spectral parameters. This method, known as the saturation-based (SB) approach, was successfully applied to several cases of sea-swell combinations and outperformed the Komen-type approaches (van  
60 der Westhuysen et al., 2007, hereafter W007; Mulligan et al., 2008). However, these applications were mostly implemented for settings with limited fetch lengths, such as lakes, bays, and small coastal areas, and shorter study periods, so that time variations of the wind field were not considered.

Other than W007 and Mulligan et al. (2008), studies that address the direct comparison between the Komen-type and SB whitecapping formulations based on real regional simulations are rare. A recent study by van Velder et al. (2016)  
65 for the North Sea during the severe storm of December 2013 showed that the Komen-type method with default parameters as incorporated in SWAN performed slightly better in the simulation of wave height, period, and frequency spectra than the SB method. This conclusion contradicts the results of previous studies. Although van Velder et al.



(2016) examined spatial and temporal variations of source terms regarding different whitecapping approaches, no specific reason was given to explain the better performance of the Komen-type formulation. The vast area of the simulation, with fetch lengths over 1000 km from the model boundary to the coastal areas where model results were evaluated, and the time variations of the wind field, are significant differences of this study from those of W007 and Mulligan et al. (2008). Hence, more studies are needed to determine the appropriate ranges of application for each whitecapping method. Moreover, wave growth and dissipation can be significantly affected by variabilities in the wind speed and direction (gustiness), instabilities in the air-sea boundary layer because of air-sea temperature difference, and slanting fetches over the coastal areas (Ardhuin et al., 2007; Donelan et al., 1985). Numerical tests of Ardhuin et al. (2007) showed that introducing wind speed gustiness may increase the simulated wave energy by up to 50%. They also reported that 10° of variability in wind direction might produce a similar effect that 10% variability in the wind speed causes. For smaller values of non-dimensional fetch, it was shown that a specific formulation of Komen-type whitecapping was generally able to reproduce the measured fetch-growth curves of Kahma and Calkoen (1992) and Walsh et al. (1989) after correction for wind direction variability as well as the instability induced by the air-sea boundary layer.

In the present study, the performance of these two whitecapping formulations is evaluated against in situ observations using simulations for the U.S East Coast coastal ocean. Wind and wave fields over this area follow a seasonal pattern with most energetic wind wave events in late fall and early winter (Allahdadi et al., 2018). During the summer, the effect of swell waves with longer periods is more pronounced over the study area, an additional component that may cause differences in the performance of Komen-type and SB whitecapping approaches. Hence, a separate model performance evaluation for each season is warranted. The present paper is dedicated to implementing this evaluation during January as the representative case for the energetic fall-winter season.

## 2 Source term quantification for whitecapping and wind input

The default approach for quantifying whitecapping dissipation in SWAN is the pulse-based, quasi-linear model of Hasselmann (1974) that was formulated by Komen et al. (1984):

$$S_{ds,w}(\sigma, \theta) = -C_{ds} \left( (1 - \delta) + \delta \frac{k}{\tilde{k}} \right) \left( \frac{\tilde{S}}{\tilde{S}_{PM}} \right)^p \tilde{\sigma} \frac{k}{\tilde{k}} E(\sigma, \theta) \quad (2)$$

$$\tilde{S} = \tilde{k} \sqrt{E_{tot}} \quad (3)$$

where  $C_{ds}$  is the whitecapping coefficient,  $\delta$  is a parameter for adjusting wave period that varies between 0 and 1 (with the default of 1 in SWAN),  $p$  is a constant,  $k$  is wave number with the average of  $\tilde{k}$ ,  $\sigma$  is the angular wave frequency with the average of  $\tilde{\sigma}$ ,  $E_{tot}$  is the total energy of the wave spectrum,  $\tilde{S}$  is the mean spectral steepness, and  $\tilde{S}_{PM} = (3.02 \times 10^{-3})^{1/2}$  is the mean spectral steepness due to the Pierson-Moskowitz spectrum (SWAN, 2015). Average angular frequency and average wave number are calculated by integration over the frequency-directional spectrum as  $E_{tot} / \iint \sigma^{-1} E(\sigma, \theta) d\sigma d\theta$  and  $\left[ E_{tot} / \iint k^{-\frac{1}{2}} E(\sigma, \theta) d\sigma d\theta \right]^2$  respectively. The strong dependency of the



formulation to the mean spectral parameters is maintained through  $\bar{k}$ ,  $\bar{\sigma}$ , and  $\bar{S}$ . Two sets of values for  $C_{ds}$  and  $p$  were found by Komen et al. (1984) and Janssen (1992) by balancing the energy equation through fetch growth tests. The Komen-type whitecapping method is conjugated with a wind input term that includes both linear and exponential growth terms (SWAN, 2015):

$$105 \quad S_{in}(\sigma, \theta) = A + BE(\sigma, \theta) \quad (4)$$

In SWAN, the linear term (A) is estimated by a formulation of Cavaleri and Malanotte-Rizzoli (1981). The exponential growth term (the term including the coefficient B) is a function of the spectral energy and accounts for the main energy input by the wind. The coefficient B for Komen et al. (1984) is calculated based on the wave age inverse  $\frac{u_*}{c}$  and angular frequency:

$$110 \quad B = \max \left[ 0, 0.25 \frac{\rho_a}{\rho_w} \left( 28 \frac{u_*}{c} \cos(\theta - \theta_w) - 1 \right) \right] \sigma \quad (5)$$

Where  $u_*$  is the wind shear velocity,  $c$  is wave phase speed,  $\rho_a$  and  $\rho_w$  are air and water densities respectively,  $\theta$  is the direction of spectral component for which wind input is calculated, and  $\theta_w$  is the wind direction.

The SB method for resolving whitecapping dissipation was developed in response to shortcomings in Komen-type methods due to the dependency of this process on the mean spectral parameters. The attempts mostly focused on removing the dependency on the mean spectral steepness and wave number. Alves and Banner (2003) presented a new form that related the wave groups to the whitecapping dissipation. This form was adopted and modified by W007 and was incorporated into SWAN as the SB model for whitecapping. This approach assumes that whitecapping dissipation affects wave groups when reaching a specific threshold:

$$120 \quad S_{ds,break}(\sigma, \theta) = -C_{ds} \left[ \frac{B(k)}{B_r} \right]^{p/2} [\tanh(kd)]^{\frac{2-p_0}{4}} \sqrt{gk} E(\sigma, \theta) \quad (6)$$

$$B(k) = \int_0^{2\pi} c_g k^3 E(\sigma, \theta) d\theta \quad (7)$$

$$p = \frac{p_0}{2} + \frac{p_0}{2} \tanh \left[ 10 \left( \sqrt{\frac{B(k)}{B_r}} - 1 \right) \right] \quad (8)$$

In the above equations,  $p_0$  is a function of the wave age inverse  $\frac{u_*}{c}$ ,  $d$  is water depth,  $g$  is acceleration due to gravity, and  $c_g$  is the wave group velocity.  $B(k)$  is defined as the azimuthal-integrated spectral saturation and  $B_r = 1.75 \times 10^{-3}$  is the threshold saturation level. If  $B(k) > B_r$ , waves break due to whitecapping. The dependency of the dissipation equation on group velocity and the associated saturation level for each wave group leads to separate estimation of the whitecapping dissipation for seas and swells and reduces their unrealistic interaction that significantly affects the whitecapping dissipation over different parts of the spectrum. In the version of SB whitecapping that is incorporated in SWAN, an additional term has been used for inclusion of dissipation caused by turbulence and interaction between long and short waves. Thus, the final whitecapping dissipation term is a weighted sum of the dissipation due to breaking and non-breaking waves:

$$130 \quad S_{ds,w}(\sigma, \theta) = f_{br}(\sigma) S_{ds,break} + [1 - f_{br}(\sigma)] S_{ds,non-break} \quad (9)$$



In the above equation,  $f_{br}(\sigma)$  is a function of  $B(k)$  and  $B_r$  that provides a smooth transition between the breaking and  
135 non-breaking components of the dissipation.

Finally, a consistent wind input expression that considers the exponential wave growth by wind, suggested  
by Yan (1987), is used in conjunction with the SB whitecapping approach. This expression is obtained based on the  
laboratory and field measurements that show quadratic growth for  $\frac{u_*}{c} > 0.1$  (e.g., Plant, 1982; Pierson and Belcher,  
2005) and linear growth for  $\frac{u_*}{c} < 0.1$  (Snyder et al., 1981; Hasselmann and Bösenberg, 1991):

$$140 \quad B = D \left( \frac{u_*}{c_{ph}} \right)^2 \cos(\theta - \theta_w) + E \left( \frac{u_*}{c_{ph}} \right) \cos(\theta - \theta_w) + F \cos(\theta - \theta_w) + H \quad (10)$$

where  $D$ ,  $E$ ,  $F$ , and  $H$  are coefficients of the fit (W007).

### 3 Modeling domain and field data

The modeling area includes the U.S East Coast from the Gulf of Maine to south Florida and the offshore areas west  
145 of  $61.0^\circ$  W (Figure1). This area is characterized by seasonal variations of winds (Allahdadi et al., 2018). During the  
late fall and the entire winter, the study area, especially the northern part, is significantly affected by extratropical  
storms with strong westerly winds that generate coastal and offshore waves with the general direction of west to east  
(Allahdadi et al., 2018). In the present study, the evolution of waves is investigated during January 2009.

The performance of the two whitecapping methods was evaluated at four NDBC buoys, including two in the north  
150 part of the modeling area (44017 nearshore and 44011 offshore) and two in the south (41004 nearshore and 41048  
offshore) (Figure 1 and Table1). Wave height, peak wave period, mean wave period, wind speed, frequency spectra,  
and other met-ocean parameters were collected at these buoys.

Time variations of observed wind at stations in the northern and southern parts of the modeling area during January  
2009 show a dominant eastward wind direction, which was the result of a winter storm spreading over the area (Figure  
155 2). With the dominant direction of the wind from west to east, it is less likely that low-frequency swell waves from  
the Atlantic Ocean could propagate toward the U.S. East Coast. Therefore, this is an ideal period to investigate the  
performance of each whitecapping approach based on the traditional fetch-limited framework. Model performance  
can be evaluated for both short and long fetch lengths. In both the northern and southern regions of the model domain,  
wind speeds of 20 m/s or larger were observed. The average wind speeds during this month were 9.7 m/s for station  
160 44011 and 8.9 m/s for 41048.

### 4 Model setup

A high-resolution unstructured SWAN model with coastal resolution of 200 m was developed and applied in this  
study. Details of the model set up are given in Allahdadi et al. (2018). Model bathymetry was prepared using two data  
165 sources, including a high-resolution database from NOAA's Coastal Relief Model with a spatial resolution of 3 arc-  
sec ( $\sim 90$  m) for the coastal areas and NOAA's ETOPO1 Global Relief Model with a spatial resolution of 1 min ( $\sim 1700$



m) for deep and offshore areas. The model was forced by wind fields from the NCEP Climate Forecast System Reanalysis (CFSR) with a spatial resolution of  $0.312^\circ$  (almost 32 km for the East Coast region) and temporal resolution of 1 hour. Evaluation of CFSR wind fields at the buoys showed the high accuracy of CFSR model outputs, especially  
170 in the offshore area (Allahdadi et al., 2018). Three-hourly snapshots of CFSR wind fields before two reference times ( $t_1$  and  $t_2$ ) are shown in Figure 3. Times  $t_1$  (1/8/2009 12:00) and  $t_2$  (1/21/2009 06:00) correspond to storms in the northern and middle parts of the model, respectively. At time  $t_1$ , a severe extratropical storm (wind speed  $> 17$  m/s) spread over the modeling area north of  $36^\circ$  N, while at time  $t_2$  the storm affects coastal and offshore areas from New York to Florida. These two reference timesteps will be used for further examination of model results in next sections.  
175 Along the open boundaries, the model was forced using the wave parameters obtained from a global WAVEWATCHIII model with a spatial resolution of  $0.5^\circ$  and temporal resolution of 3 hours. Following Whalen and Ochi (1978), Ochi (1998), and Allahdadi et al. (2004b), a JONSWAP frequency-spectra with the average enhance parameter of  $\gamma=3.3$  was chosen for converting parametric wave data to 2-D spectra along the boundary. Due to the dominant west-to-east wind over the modeling area during the simulation period, it is less likely for boundary waves  
180 to propagate toward the modeling area. Nevertheless, realistic boundary data were used in this study. The number of spectral directions and frequencies for discretization of 2-D spectra were 24 and 28, respectively. Simulation was done using a minimum frequency of 0.04 Hz, maximum frequency of 1.00 Hz, and a computational time step of 10 minutes (Allahdadi et al., 2018). Source terms for whitecapping dissipation and their associated wind input formulation were examined based on the two types of whitecapping dissipation approaches discussed in section 2. For the rest of source  
185 terms including quadruplets, triads, depth-induced wave breaking, and bottom dissipation, the default methods in SWAN were used.

## 5 Results

Based on the model setup described in section 4, twin simulations were performed for January 2009 using Komen  
190 (1984) and van der Westhuysen (2007) to supply the formulation for quantifying whitecapping dissipation (Komen and Westhuysen hereafter). For both approaches, only the default SWAN parameters were used. Simulated wave height and mean period ( $T_{02}$ ) for both approaches were compared with measurements at NDBC stations 41004, 41048, 44017, and 44011 (Figure 4). Comparisons with field data show that both whitecapping approaches underestimate wave height and wave period (less pronounced for Komen) at all stations. For all stations, Westhuysen simulated  
195 smaller wave heights compared to both observations and Komen. (Figures 4a to 4d). While at all four stations Westhuysen significantly underestimates the wave period (Figures 4e to 4h), wave periods from Komen differed from observations at some stations. Comparison results for wave height and period as obtained from measurements and simulation scenarios for  $t_1$  and  $t_2$  show similar patterns (Table2).

Simulation results for two whitecapping methods compared to buoy measurements are further investigated through  
200 scatter plots (Figures 5 and 6). Comparisons are quantified using standard metrics for model performance including correlation coefficient (R), bias, root mean square error (RMSE), and scatter index (SI) (Tehrani et al., 2013; Chaichitehrani et al., 2014; Yang et al., 2017). Statistics for wave height show that while the correlation coefficient



of the match-up comparison is slightly larger for the Westhuysen, at all four buoys, the average errors of the simulated wave heights (bias) and the average distance from the ideal agreement line (RMSE) are significantly smaller for Komen (Figure 5). The only exception is the RMSE for buoy 44017, for which the corresponding value of RMSE from Komen is just slightly larger than that of Westhuysen (0.52 for Komen and 0.49 for Westhuysen, see Figure 5c). Scatter indices, which show the scattering of simulated values around the ideal match-up line, are smaller at buoys 41004, 41048, and 44011 for simulated wave heights by Komen. Again, the exception is buoy 44017. This different behavior could be due to the complex coastal geography upwind of the station that causes the slanting fetch effect when the prevailing wind is from the land toward offshore (Ardhuin et al., 2007). This effect will be further examined in Section 6. For simulated mean wave periods, the correlation coefficients between the two scenarios are very similar at all buoys (Figure 6). However, the remaining performance statistics significantly favor the Komen whitecapping predictions. For all buoys, Westhuysen substantially underestimates the mean wave period with the RMSE values between 1.1 and 1.6 seconds, while for the Komen method, RMSEs range between 0.85 to 1.05 seconds.

Simulated wave heights and periods using Komen and Westhuysen whitecapping approaches at times t1 and t2 are also investigated by examining snapshots of results over the modeling area (Figure 7). At time t1, significant differences are observed between wave heights from the twin simulations, especially within the extensive region in the north that was affected by the intense storm winds (Figures 7a and 7b). Similarly, at timestep t2 (Figures 7c and 7d), significant differences result for the extensive areas offshore of North Carolina to New Jersey that is close to the instantaneous center of the storm. At both t1 and t2, substantial differences are observed between simulated wave periods (Figure 7e to 7h). At t1 (Figures 7e and 7f), wave periods off the New York coast are significantly underestimated by Westhuysen compared to Komen (period of 7 sec for Westhuysen and 9 sec for Komen), a pattern that is also observed for time t2 (Figures 7g and 7f) for all offshore areas off the Florida to Massachusetts coast.

To examine the performance of each whitecapping approach in the simulation of wave energy distribution, frequency spectra from two experiments were compared with measured spectra at each buoy and for t1 (Figure 8) and t2. Hourly frequency spectra at the buoys are available from observations for the frequency band of 0.02-0.485 Hz. However, spectral energy corresponding to frequencies smaller than 0.06 Hz were zero. To minimize the effect of measurement noises at t1 and t2, measured spectra were averaged within a three-hour time window. At each location, frequency spectra were also presented in semilogarithmic scale on the energy axis to more clearly show the differences.

At t1 at buoy 41011, both methods appropriately simulated the general shape of the single-peaked spectrum and the value of the peak frequency (a slight overestimation by Westhuysen for peak frequency). While Komen simulated an almost identical peak energy, Westhuysen underestimated it by 18%. The peak of energy is also maintained by Komen for the other offshore station (NDBC 41048), but with significant underestimation of the peak frequency in the simulated spectra (about 30%). For both coastal stations (44017 and 41004), the peak of energy is significantly underpredicted by both experiments (34-75% depending on the station and simulation experiment) while the peak frequencies were off by -15 to 23%. At all buoys, Komen simulated larger peaks of energy, which are closer to the measurements. The consistency of the simulated frequency spectra at 44011 with that of measurements at time t1 could be due to the persistent winds with almost constant speed and direction from the coast toward the station at this



time and several hours before it (at least 6 hours; Figure 3). This wind condition can produce the fetch-limited wave growth with the well-developed single-peaked spectrum (Hasselmann et al., 1973) that can likely be simulated by different whitecapping formulations because they are evaluated and calibrated mainly based on the measured fetch-limited growth curves (W007, Ardhuin, et al. 2007). Discrepancies at the two coastal stations could be caused by the effect of land roughness on the CFSR wind over the coastal areas (Allahdadi et al., 2018), non-persistence of wind field over these areas, and effect of slanting fetch (Ardhuin et al., 2007). The fetch-limited wave growth at 44011 is of particular interest due to available field observations and modeling studies (for instance, Kahma and Clyson, 1994). As mentioned above, at this station at t1 the Komen approach shows almost identical values for the peak of energy and peak frequency to the measurements, while Westhuysen underestimates the peak of energy and overestimates the peak frequency. These results are in contradiction to the simulation result of W007 for a wave evolution test off the coast of North Carolina, USA. Their result showed that in the absence of offshore swells, the SB approach (Westhuysen) simulated higher levels of spectral energy corresponding to the peak frequency than that of Komen. Also, the simulated peak frequency from the SB model was more consistent with measurements. These different behaviors could be due to different growth conditions and wave age stages discussed in the next section.

Similar patterns for comparison of simulated frequency spectra based on twin simulations and measurements are observed at time t2 (not shown). Because at this time the most persistent winds occur in the middle part of the modeling area, NDBC41048 shows the best consistency for spectral energy and peak frequency.

## 6 Discussion

### 6.1 Examining source terms

Simulation results presented in the previous section clearly show that compared to the in situ observations, the Komen whitecapping approach results in higher accuracy for both wave height and period. Over the modeling area, especially close to the instantaneous center of the storms at times t1 and t2, simulated wave heights and periods from Komen are larger than those of Westhuysen.

Spatial and temporal variations of source terms for wind input ( $S_{wind}$ ), whitecapping dissipation ( $S_{wc}$ ), and quadruplet ( $S_{nl_4}$ ) were obtained from SWAN simulations and diagnosed at these two times for both simulations to illustrate the contribution of source terms in the simulation results (Figure 9). For each modeling simulation, the three essential source terms are of the same order of magnitude and show similar values. This is consistent with Bouws and Komen (1983) and van Vledder et al. (2016). The quantified source terms by Westhuysen are significantly larger than those of Komen. For example, off the coast from New York Harbor to the Gulf of Maine, the estimated  $S_{wind}$  by Komen varies between  $1.5 - 2 \times 10^{-4} \text{ w/m}^2$  (except a small higher energy zone in the very northeast edge) whereas the simulated wind input source term by Westhuysen approach is at least twice as large as Komen's. This is because the wind input term is a direct function of  $\frac{u_*}{c}$  in both formulations, but the wind input formulation for Komen (equation 5) is a linear function of this parameter and is mostly appropriate for weaker wind speeds up to 12 m/s (W007). Conversely, the wind input associated with Westhuysen whitecapping (Yan, 1987; equation 10) is appropriate for both



275 weak and strong wind forcing and includes generation of wind energy as a function of both  $\frac{u_*}{c}$  and  $(\frac{u_*}{c})^2$ . The wind  
input formulation for each whitecapping approach has been selected to be consistent with the scaling of the  
whitecapping to appropriately simulate the observed shape of the evaluated frequency spectra (W007). Particularly  
for the spectral tail with frequencies 1.5 times higher than the peak frequency, Resio and Perrie (1991) reported that  
the dominant shape of the spectrum is a form which is a function of  $f^{-4}$  ( $f$  is wave frequency) for both weakly and  
280 strongly forced waves. This shape results from the stabilizing effect of the quadruplet interactions. Hence, spatial  
variations of whitecapping dissipation for each approach are of the same order of magnitude as their wind input  
counterpart. Similar to the wind input, the simulated whitecapping using Westhuysen shows higher values than those  
simulated by Komen. Compared to wind input and whitecapping, estimated quadruplet source terms by Komen and  
Westhuysen are closer in value.

285 Estimated source terms from the two simulations were also compared by examining variations in the frequency space  
at buoy 44011 at t1 (Figure 10). In addition to the main source terms of wind input, whitecapping dissipation, and  
quadruplet, their algebraic sums (sum of the first three right-hand terms in equation 1) are also compared in the  
frequency domain. Like the integrated values of these source terms over the modeling area (Figure 9), variations of  
source terms versus frequency show larger values of wind input and stronger whitecapping dissipation by the  
290 Westhuysen approach (Figures 10a and 10b). The algebraic sum of the source terms is the ultimate energy amount  
that is produced at each time step due to source term interactions and is subjected to spatial and temporal variations  
based on the equation of wave action conservation. Hence, variations of this term in the frequency domain can be  
consistent with the shape of the energy-frequency spectra of Figure 8. Komen simulated a larger sum of source terms  
at the peak frequency and all frequencies below that (Figure 10d). This result is consistent with Figures 8a that shows  
295 higher spectral energies at this time by Komen compared to Westhuysen. The consistent spectral energies from Komen  
and Westhuysen for the high-frequency spectral tail in Figure 8 can also be explained using Figure 10d. Compared to  
the peak frequency, simulated sums of source terms for frequencies larger than the peak frequency are half or smaller  
and their difference is not large enough to cause different spectral shapes in the tail of spectra.

## 300 6.2 Effect of wind field and growth conditions

In this section, the deficiencies associated with the Komen and Westhuysen whitecapping methods are investigated  
based on wave growth conditions during the simulation period. The performance of these two approaches for  
quantifying whitecapping dissipation and their wind input counterparts highly depends on the spatial and temporal  
variations of the wind field and the spatial scale of the modeling area, which both affect wave growth. Hence,  
305 developed approaches for wind input and whitecapping are primarily calibrated and verified using observed growth  
curves. These growth curves are represented in the form of non-dimensional energy and non-dimensional frequency  
both versus non-dimensional fetch  $X^* = gX/u_*^2$  where  $X$  is the fetch length. W007 verified both the SB (Westhuysen)  
and Komen (using the default SWAN parameters like the present study) whitecapping approaches versus the growth  
curves of Kahma and Calkoen (1992) (for fetch-limited growth) and Pierson-Moskowitz (1964) (for the fully-  
310 developed sea state) and determined the default calibration parameters for the SB model. The comparisons showed



that using the default parameters for whitecapping, both approaches performed well during the fetch-limited growth when the value of the non-dimensional fetches are  $<10^7$ , although for  $X^*$  values between  $10^4$  and  $10^5$ , the Westhuysen approach was more consistent with observations. This study also indicated that for the fully-developed part of the growth curve ( $X^* > 10^7$ ), the Komen approach with default parameters simulated higher amounts for the non-dimensional energy than Westhuysen. Although simulated non-dimensional energy by Komen was more consistent with observations, both approaches underestimated it. Furthermore, both whitecapping approaches overestimated the non-dimensional peak frequency for  $X^* > 10^7$  that leads to lower wave periods in simulation. These cases of inconsistency could partly contribute to the underestimation of wave height and period obtained from Komen and Westhuysen whitecapping approaches with default parameters. Among the four NDBC buoys used for model result verification in this study, two (41011 and 41048) are offshore 600 and 1300 km from the shoreline in the east-west direction. Hence, because of the dominant offshore-ward direction of the wind during the simulation period in January 2009 (Allahdadi et al., 2018), large values for the non-dimensional fetch could result at these locations. This could be corresponding to the fully-developed sea state that is the zone of inconsistency based on the above discussions. At t1, a strong wind with a westerly direction affected the East Coast and offshore areas north of  $33^\circ\text{N}$ . The consistent wind direction with the average speed of about 15.5 m/s from the coast to buoy 41011 produced a fully-developed sea state with  $X^* \approx 2 \times 10^7 > 10^7$ . Hence, underestimation in both wave height and wave period is expected. However, in this area of the growth curve, Komen generates higher levels of energy, i.e. higher wave heights result (Figure 4). For the other offshore station (41048), even larger values for  $X^*$  on the order of  $10^8$ - $10^9$  are obtained that correspond to larger underestimations that are also evidenced in Figure 4. At t2 and 6-10 hours before that, the wind at buoy 41011 was consistently from the northeast with average speed of 7 m/s, corresponding to a strong fully-developed sea state with  $X^* \approx 10^8$ . At this time, the wave height was significantly underestimated by both whitecapping approaches, especially by Westhuysen (Table 2). At coastal stations, however, due to the generally short fetch lengths during the winter storm outbreak, fully-developed sea states were less likely. For instance, at both t1 and t2, the persistent wind at buoy 41017 corresponded to  $X^* = 5 \times 10^6$  and  $4.3 \times 10^6$  respectively indicating fetch-limited growth.

Wind input and whitecapping source terms for both Komen and Westhuysen are direct or indirect functions of the wave age inverse  $\frac{u_*}{c}$  (equations 5, 8, and 10). Multiple studies reported that with increasing wave age (decreasing the wave age inverse), dissipation due to whitecapping decreases (W007; Longuet-Higgins and Smith, 1983; Katsaros and Ataktürk, 1992). Wave age inverse is also an appropriate manifestation of the sea state and an indicator of whether the sea state is in the forcing phase or fully-developed. Volov (1970) and Oost (1998) suggested and Drennan and Graber (2003) later confirmed that a developing sea corresponds to  $\frac{u_*}{c} > 0.05$ , while  $0.033 < \frac{u_*}{c} < 0.05$  indicates a fully-developed sea state. For offshore buoy 44011 and nearshore buoy 44017, variations of simulated hourly whitecapping dissipation with the inverse wave age for two experiments are plotted in Figure 11. Since the scaling of the whitecapping formula in Komen and Westhuysen differ (Figure 9), simulated whitecapping values on the vertical axes are normalized based on the maximum value in each case. At both stations and for both whitecapping methods, whitecapping dissipation increases with increasing inverse wave age, although the nearshore station has more scattering, presumably due to the fetch length variations caused by the coastline irregularities. At the offshore station



41011(Figures 11a and 11c), significant numbers of events are included in the fully-developed zone. The density of the simulated incidents in this zone decreased for the coastal station due to smaller fetch lengths.

350 The above discussion shows that for the East Coast, a significant part of the deficiencies at offshore buoys (and to some extent at nearshore buoys) could be caused by the spectral energy underestimation/peak frequency underestimation by these approaches during fully-developed sea states. This could be fixed by revisiting the models' calibration process and selecting smaller amounts for the default whitecapping parameter ( $C_{dis}$ ) corresponding to the large values of the non-dimensional fetches. The default value for Komen whitecapping as presented by Komen et al. (1984) is  $2.3 \times 10^{-5}$ , while for the Westhuysen approach, W007 suggested  $C_{dis} = 5 \times 10^{-5}$  based on comparisons  
355 with field measurements. However, the modified whitecapping parameter for the fully-developed condition may cause inconstancies in the fetch-limited zone of the growth-curve regarding the fact that the simulated non-dimensional energies and peak frequencies already match the measurements. Hence, it is suggested that in future modifications, fully-developed and fetch-limited conditions are treated independently, so that models could be able to calculate the whitecapping parameters based on the instantaneous non-dimensional fetches. Furthermore, within an extensive  
360 modeling area with a high spatially and temporally variable wind field, an ideal fetch-limited condition is less likely to occur, at least for offshore areas, for the East Coast during winter storms. The large fetch lengths for these areas need several hours of persistent winds with small variations in speed and direction to develop a fetch-limited condition. However, spatial and temporal variations of the wind field over this area cannot generally stimulate such a condition. In fact, times  $t_1$  and  $t_2$  were two infrequent cases for which the persistent winds were dominant over a part of modeling  
365 area for several hours. It means that for many points on Figure 11, the values of  $\frac{u_s}{c} > 0.05$  may represent duration-limited wave growth that is not a part of the calibration process during the development of the whitecapping approaches, especially for Westhuysen. Revisiting the calibration process and including the duration-limited growth curves (non-dimensional wind duration instead of non-dimensional fetch) can lead to updated and more consistent calibration parameters. For coastal buoys, the coastal geometry may influence model accuracy as discussed in the next  
370 section.

### 6.3 Effect of coastal geometry

Similar to the offshore regions, deviations from the fetch-limited condition in coastal areas can contribute to the underestimation of wave height and period, although due to shorter fetch lengths it is more likely for the coastal areas  
375 to reach fetch-limited growth. However, significant underestimation for both wave height ( $0.32 < RMSE < 0.52$  m) and period ( $0.85 < RMSE < 1.37$  sec) were observed from simulation results at the two coastal stations (41004 and 44017; see Figures 5 and 6 for details). Due to relatively deep water at these locations (38 and 52 m respectively), shallow water phenomena are not likely to affect simulation results. However, the proximity to land may contribute to the underestimation in several ways. First, although the 32 km spatial resolution of CSFSR wind that was used for  
380 the present simulation is one of the finest available resolutions for the East Coast, interpolation of wind land points over the mesh in the coastal areas may significantly underestimate wind speed used in SWAN. Second, regarding the performance of whitecapping and wind input approaches over the coastal areas, several studies highlighted the effect



of the fetch geometry and the deviation of the wind direction from the shore-normal direction on wave evolution (e.g., Arduin et al., 2007; Donelan et al., 1985). Arduin et al. (2007) used the term “slanting fetch” for such a condition.

385 Based on wave measurements at several coastal stations along the North Carolina and Virginia coast, they observed that even with small deviations in offshore-ward wind direction from the shore-normal, two distinct wind-sea systems are produced. The low-frequency systems propagate alongshore in the approximate direction of the slanting fetch, while the higher frequency wave system propagates downwind. Observed frequency-directional spectra at buoy 44017 at t1 and t2 (Figures 12a and 12b) illustrate this behavior. From a modeling perspective, whitecapping approaches and

390 their wind input counterparts may fail partly or entirely to simulate the part of the spectra with higher directional spreading from the mean wind direction (Arduin et al., 2007). Arduin et al. (2007) reported that the directional distribution associated with the wind input term of Jensen (1991) is too narrow and is not able to simulate enough energy for directional bands away from the mean wind direction. Consequently, less energy is transferred to the directions close to the slanting fetch compared to observations and this may contribute to a further underestimation of

395 wave height and period at the location of coastal stations. The simulated frequency-directional spectra at buoy 44017 using Komen and Westhuysen approaches at t1 and t2 are compared with those from observations in Figure 12 c-f. At t1, the local wind direction is from west to east, and the measured spectrum (Figure 12a) shows a wide spectral band extended from 90 to 300 in the clockwise direction with the high energy zone formed at directions close to the wind direction. At the same time, a lower frequency spectral band from 330 to 85 with the main direction parallel to the

400 coastline (Long Island is to the north of 44017) is produced as a separate wave system. The simulated wave spectra using both whitecapping approaches, however, capture only the higher frequency portion of the spectrum generated downwind and fail to simulate the lower frequency part produced by the slanting fetch effect. While their directional spreading is almost the same (Komen’s spectra is slightly wider), as expected, Komen results in higher energy levels. Although at t2 simulated spectra were able to reproduce the main portion of the low-frequency spectral zone caused

405 by the slanting fetch effect, they both failed to include that portion of the low-frequency wave system that propagated from the northern quadrant (Figures 12 d and 12f).

#### 6.4 Effect of boundary layer instability

For both Komen and Westhuysen approaches, the associated wind input terms are quantified by assuming a stable air-sea boundary layer, i.e., air temperature is assumed to be the same as or higher than the sea surface temperature.

410 However, there are many occasions, especially during the winter, when the air is colder than the water. This negative temperature difference can cause instability at the air-sea boundary layer and lead to higher rates of wind energy transfer to the water surface. This instability effect has been studied by several researchers to modify the quantification of the wind input source term (e.g., Abdalla and Cavaleri, 2002; Tolman, 2002). Tolman (2002) suggested a

415 relationship for correcting wind speed based on the air-sea temperature difference that increases the input wind speed to the model if this difference is negative. Arduin et al. (2007) applied this relationship to an unstable case with  $dT = -10$  ( $dT = \text{air temperature} - \text{water temperature}$ ) to correct the wind speed and were able to successfully reproduce the unstable growth curve of Kahma and Calkoen (1992). For this amount of the air-sea temperature difference, Tolman’s relationship showed about a 24% increase in the input wind speed compared to the neutral case. Field measurements



420 of air temperature and sea surface temperature at different locations in the model domain showed that during the  
simulation period in January 2009, there were many events with an unstable boundary layer. These instability incidents  
are more frequent and stronger for buoys in the north of the model domain (Figure 13a for 44011). To illustrate the  
potential effect of temperature instabilities on simulation results, observed and simulated wave heights based on both  
simulations are presented in Figure 13b. For most days during January 2009, the air-sea temperature difference was  
425 negative, indicating an unstable boundary layer. Temperature differences were as low as  $-10^{\circ}\text{C}$  with the average of  $-5^{\circ}\text{C}$ ,  
corresponding to an increase in wind speed from 15-24% based on Tolman's relationship. In the present  
simulation, wind speed correction due to the boundary layer instability was not considered. As shown in Figure 13b,  
the underestimation of wave height by both whitecapping approaches in many cases coincided with the negative  
temperature difference occurred several hours to 1-2 days before the peak of wind/wave. Hence, by incorporating  
430 appropriate modifications that include the effect of boundary layer instability on the wind field, higher wave heights  
that are more consistent with observations are expected.

## 7 Summary and Conclusion

Selecting appropriate modeling approaches for wind input and whitecapping source terms is essential for high  
435 accuracy wave modeling. Available methods have some limitations regarding the wind climate over the modeling  
area, spatial scales, coastal geometry, and presence of swell waves. The Komen-type whitecapping methods produce  
spurious results under a combination of seas and swells. The SB model of W007 (Westhuysen) was developed to  
modify this spurious effect. For an extensive modeling area like the U.S. East Coast and its offshore areas, the  
performance of each type of whitecapping method and its associated wind input terms should be evaluated during  
440 varied meteorological conditions. Since the wind conditions of the East Coast are very different between winter  
and summer, seasonal investigations need to be done separately. During the winter, wind direction is mostly offshore-  
ward and along the coast, and Atlantic swells are less likely to propagate over the model domain, while during the  
summer, wind power significantly weakens and swell waves predominate.

The present paper evaluates model performance during an outbreak of winter storms in January 2009. Simulation  
445 results showed that using either Komen or Westhuysen to resolve whitecapping led to an underestimation of wave  
height at coastal and offshore stations, although Komen resulted in larger wave heights that were more consistent with  
observations. While simulated mean wave periods using Komen were in a good agreement with observations,  
Westhuysen significantly underestimated wave periods at all four buoy locations used for model evaluation.  
Examining the quantified source terms over the modeling area indicated that for each whitecapping approach, the  
450 source terms for wind input, whitecapping dissipation, and quadruplet have the same order of magnitude and follow  
similar spatial and temporal variations. For the wind input formulation of Yan (1987), which is associated with the  
Westhuysen whitecapping method, the wind input source term was modified for the intense wind speeds that include  
the energy generation as a function of both  $(\frac{u_*}{c})^2$  and  $\frac{u_*}{c}$ . Hence, the resulting wind input at the peak of the storm was  
2-3 times larger than that of Komen, which only scales the wind input as a linear function of  $\frac{u_*}{c}$ . For both methods,  
455 quantification of the whitecapping dissipation terms (and thereby calculation of the quadruplet term) accords with the



scaling of the wind input terms. The algebraic sum of source terms (that is transferred to the equation for the conservation of the wave action density) from Komen includes higher amounts of energy, especially for lower frequencies and at peak frequency. This leads to higher spectral energies from Komen whitecapping available to the frequency-directional spectra that contributes to larger wave heights and periods compared to Westhuysen. Several reasons contribute to this underestimation over the coastal and offshore areas. Generally, the whitecapping formulas and their wind input counterparts are developed and tested to comply with the traditional fetch-limited and fully-developed growth curves. For the specific case of the saturation-based whitecapping and to some extent Komen-type whitecapping, the numerical tests of W007 showed that the calibrated models based on default parameters underestimate spectral energy within the fully-developed part of the growth curve. This behavior corresponds to the underestimation of wave height and period at the offshore buoys, where the large fetches during the offshore-ward wind events are more likely to produce fully-developed growth compared to coastal stations. For many events that do not correspond to the fully-developed sea state at the offshore and coastal stations, wave parameters are still underestimated. This could be partly because of the transient wind field that produces duration-limited growth, a condition that was not included in the calibration and verification of whitecapping approaches during their development phase. Therefore, re-visiting the calibration process for both methods and representing new default parameters for whitecapping is highly recommended. The default parameters should be presented for different wave development conditions including fetch-limited, duration-limited, and fully-developed. The duration-limited condition should be especially considered since it has not been included in previous studies of developing and testing the whitecapping methods.

For the coastal stations, the deviation of the wind direction from the shore-normal direction that is very likely due to the complicated coastal geometry and significant temporal and spatial variabilities of the wind field, causes the “slanting fetch” effect that transfers part of the wind-induced energy to the low frequencies and wave propagation along the shoreline. Since the wind input formulations generally are not able to simulate large spreading from the mean wind direction, this alongshore counterpart of the 2-D spectra may be overlooked by models. Comparison with observed 2-D spectra at coastal stations showed that both whitecapping approaches partly or completely fail to include this low frequency part, further contributing to the underestimation of wave parameters.

Instabilities in the air-sea boundary layer induced by colder air temperature than sea surface temperature may significantly increase wind energy transfer to waves, i.e., create larger wave heights. Although during January 2009, this temperature difference at the offshore station 44011 reached  $-10^{\circ}\text{C}$ , none of the wind input approaches are able to include this intensifying effect.

In the present study, low frequency swell waves from the Atlantic were less likely to propagate toward the modeling area under the prevailing west-to-east wind direction. Hence, the evaluation was mostly limited to the pure wind-wave generation. More studies are required to address the spurious effect of low-frequency swell waves on whitecapping dissipation resulting from the Komen-type models over this study area. Therefore, similar simulations and analyses for the summer will be conducted. Results will be reported in future correspondence.



## 8 Acknowledgments

This study was funded by the Wind and Water Power Technologies Office (WWPTO) within the Office of Energy Efficiency and Renewable Energy (EERE), U.S. Department of Energy. Sandia National Laboratories is a multi-  
495 mission laboratory managed and operated by National Technology and Engineering Solutions of Sandia LLC, a wholly owned subsidiary of Honeywell International Inc. for the U.S. Department of Energy's National Nuclear Security Administration under contract DE-NA0003525. This paper describes objective technical results and analysis. Any subjective views or opinions that might be expressed in the paper do not necessarily represent the views of the U.S. Department of Energy or the United States Government. RH also acknowledges research support  
500 provided by NSF grant OCE1559178 and NOAA grant NA11NOS0120033. We thank Jennifer Warrillow for editorial assistance with the manuscript

## References

- 505 Abdalla, S. and Cavaleri, L.: Effect of wind variability and variable air density on wave modeling, *Journal of Geophysical Research: Oceans*, 107(C7), 17-1-17-17, doi:10.1029/2000JC000639, 2002.
- Allahdadi, M.N., Gunawan, B., Lai, J., He, R. and Neary, V.S.: High Resolution Wave modeling for Characterizing Wave Energy Resources along the U.S East Coast , Abstract [CD51A-02] presented at 2018 Ocean Sciences Meeting, Portland, OR, 12-16 Feb, 2018.
- 510 Allahdadi, M. N., Chaichitehrani, N., Allahyar, M. and McGee, L.: Wave Spectral Patterns during a Historical Cyclone: A Numerical Model for Cyclone Gonu in the Northern Oman Sea, *Open Journal of Fluid Dynamics*, 07(02), 131, doi:10.4236/ojfd.2017.72009, 2017.
- Allahdadi, M.N., Fotouhi, N. and Taebi, S.: Investigation of Governing Wave Spectral Pattern near Anzali Port Using Measured Data. Proceedings of the 6th International Conference on Coasts, Ports, and Marine Structures,  
515 Tehran, Iran, 2004.
- Allahdadi, M.N. Chegini, V., Fotouhi, N. and Golshani, A.: Wave Modeling and Hindcast of the Caspian Sea. Proceedings of the 6th International Conference on Coasts, Ports, and Marine Structures, Tehran, Iran, 2004.
- Alves, J. H. G. M. and Banner, M. L.: Performance of a Saturation-Based Dissipation-Rate Source Term in Modeling the Fetch-Limited Evolution of Wind Waves, *J. Phys. Oceanogr.*, 33(6), 1274-1298, doi:10.1175/1520-  
520 0485(2003)033<1274:POASDS>2.0.CO;2, 2003.
- Ardhuin, F., Herbers, T. H. C., Watts, K. P., van Vledder, G. P., Jensen, R. and Graber, H. C.: Swell and Slanting-Fetch Effects on Wind Wave Growth, *J. Phys. Oceanogr.*, 37(4), 908-931, doi:10.1175/JPO3039.1, 2007.
- Cavaleri, L. and Rizzoli, P. M.: Wind wave prediction in shallow water: Theory and applications, *Journal of Geophysical Research: Oceans*, 86(C11), 10961-10973, doi:10.1029/JC086iC11p10961, 1981.
- 525 Chaichitehrani, N., D'Sa, E. J., Ko, D. S., Walker, N. D., Osburn, C. L. and Chen, R. F.: Colored Dissolved Organic Matter Dynamics in the Northern Gulf of Mexico from Ocean Color and Numerical Model Results, *Journal of Coastal Research*, 800-814, doi:10.2112/JCOASTRES-D-13-00036.1, 2013.
- Donelan, M.A., Hamilton, J. and Hui, W.H.: Directional spectra of wind-generated ocean waves. *Phil. Trans. R. Soc. Lond. A* 315, 509-562. <https://doi.org/10.1098/rsta.1985.0054>, 1985.
- 530 Drennan, W. M., Graber, H. C., Hauser, D. and Quentin, C.: On the wave age dependence of wind stress over pure wind seas, *Journal of Geophysical Research: Oceans*, 108(C3), doi:10.1029/2000JC000715, 2003.



- 535 Hasselmann, D. and Bösenberg, J.: Field measurements of wave-induced pressure over wind-sea and swell, *Journal of Fluid Mechanics*, 230, 391–428, doi:10.1017/S0022112091000848, 1991.
- Hasselmann, K.: On the spectral dissipation of ocean waves due to white capping, *Boundary-Layer Meteorol*, 6(1), 107–127, doi:10.1007/BF00232479, 1974.
- 540 Hasselmann, K., Barnett, T. P., Bouws, E., Carlson, H., Cartwright, D. E., Enke, K., Ewing, J. A., Gienapp, H., Hasselmann, D. E., Kruseman, P., Meerburg, A., Müller, P., Olbers, D. J., Richter, K., Sell, W. and Walden, H.: Measurements of wind-wave growth and swell decay during the Joint North Sea Wave Project (JONSWAP), *Ergänzungsheft* 8-12, 1973.
- Janssen, P. A. E. M.: Quasi-linear Theory of Wind-Wave Generation Applied to Wave Forecasting, *J. Phys. Oceanogr.*, 21(11), 1631–1642, 1991.
- 545 Kahma, K. K. and Calkoen, C. J.: Reconciling Discrepancies in the Observed Growth of Wind-generated Waves, *J. Phys. Oceanogr.*, 22(12), 1389–1405, 1992.
- Kamranzad, B., Etemad-Shahidi, A. and Chegini, V.: Sustainability of wave energy resources in southern Caspian Sea, *Energy*, 97(Supplement C), 549–559, doi:10.1016/j.energy.2015.11.063, 2016.
- Katsaros, K. B. and Ataktürk, S. S.: Dependence of Wave-Breaking Statistics on Wind Stress and Wave Development, in *Breaking Waves*, edited by M. L. Banner and R. H. J. Grimshaw, pp. 119–132, Springer Berlin Heidelberg., 1992.
- 550 Komen, G. J., Hasselmann, K. and Hasselmann, K.: On the Existence of a Fully Developed Wind-Sea Spectrum, *J. Phys. Oceanogr.*, 14(8), 1271–1285, 1984.
- Longuet-Higgins, M. S. and Smith, N. D.: Measurement of breaking waves by a surface jump meter, *Journal of Geophysical Research: Oceans*, 88(C14), 9823–9831, doi:10.1029/JC088iC14p09823, 1983.
- 555 Mulligan, R. P., Bowen, A. J., Hay, A. E., Westhuysen, A. J. van der and Battjes, J. A.: Whitecapping and wave field evolution in a coastal bay, *Journal of Geophysical Research: Oceans*, 113(C3), doi:10.1029/2007JC004382, 2008.
- Niroomandi, A., Ma, G., Ye, X., Lou, S. and Xue, P.: Extreme value analysis of wave climate in Chesapeake Bay, *Ocean Engineering*, 159, 22–36, doi:10.1016/j.oceaneng.2018.03.094, 2018.
- 560 Ochi, M.K.: *Ocean Waves: The Stochastic Approach*. Cambridge University Press, Cambridge.  
<https://doi.org/10.1017/CBO9780511529559>, 1998.
- Oost, W. A.: The KNMI HEXMAX stress data – a reanalysis, *Boundary-Layer Meteorology*, 86(3), 447–468, doi:10.1023/A:1000824918910, 1998.
- 565 Peirson, W. L. and Belcher, S. E.: Growth response of waves to the wind stress, in *Coastal Engineering 2004*, pp. 667–676, World Scientific Publishing Company., 2005.
- Plant, W. J.: A relationship between wind stress and wave slope, *Journal of Geophysical Research: Oceans*, 87(C3), 1961–1967, doi:10.1029/JC087iC03p01961, 1982.
- 570 Resio, D. and Perrie, W.: A numerical study of nonlinear energy fluxes due to wave-wave interactions Part 1. Methodology and basic results, *Journal of Fluid Mechanics*, 223, 603–629, doi:10.1017/S002211209100157X, 1991.
- Siadatmousavi, S. M., Jose, F. and Stone, G. W.: Evaluation of two WAM white capping parameterizations using parallel unstructured SWAN with application to the Northern Gulf of Mexico, USA, *Applied Ocean Research*, 33(1), 23–30, doi:10.1016/j.apor.2010.12.002, 2011.



575

Siadatmousavi, S. M., Allahdadi, M. N., Chen, Q., Jose, F. and Roberts, H. H.: Simulation of wave damping during a cold front over the muddy Atchafalaya shelf, *Continental Shelf Research*, 47(Supplement C), 165–177, doi:10.1016/j.csr.2012.07.012, 2012.

580

Snyder, R. L., Dobson, F. W., Elliott, J. A. and Long, R. B.: Array measurements of atmospheric pressure fluctuations above surface gravity waves, *Journal of Fluid Mechanics*, 102, 1–59, doi:10.1017/S0022112081002528, 1981.

SWAN.: SWAN: User Manual, Cycle III Version 41.01A, Delft University of Technology, Delft, The Netherlands, 2015

585

Tehrani, N. C., D'Sa, E. J., Osburn, C. L., Bianchi, T. S. and Schaeffer, B. A.: Chromophoric Dissolved Organic Matter and Dissolved Organic Carbon from Sea-Viewing Wide Field-of-View Sensor (SeaWiFS), Moderate Resolution Imaging Spectroradiometer (MODIS) and MERIS Sensors: Case Study for the Northern Gulf of Mexico, *Remote Sensing*, 5(3), 1439–1464, doi:10.3390/rs5031439, 2013.

Tolman, H. L.: Validation of WAVEWATCH-III version 1.15. NOAA/NWS/NCEP/MMAB Tech. Rep. 213, 33 pp, 2002.

590

van der Westhuysen, A. J., Zijlema, M. and Battjes, J. A.: Nonlinear saturation-based whitecapping dissipation in SWAN for deep and shallow water, *Coastal Engineering*, 54(2), 151–170, doi:10.1016/j.coastaleng.2006.08.006, 2007.

Vledder, G. P. van, Hulst, S. T. C. and McConochie, J. D.: Source term balance in a severe storm in the Southern North Sea, *Ocean Dynamics*, 66(12), 1681–1697, doi:10.1007/s10236-016-0998-z, 2016.

595

Volkov, Y. A.: Turbulent flux of momentum and heat in the atmospheric surface layer over a disturbed surface, *Izv. Acad. Sci. USSR Atmos. Oceanic Phys., Engl. Transl.*, 6, 770–774, 1970.

Whalen, J. E. and Ochi, M. K.: Variability Of Wave Spectral Shapes Associated With Hurricanes, *Offshore Technology Conference.*, 1978.

600

Walsh, E. J., Hancock, D. W., Hines, D. E., Swift, R. N. and Scott, J. F.: An Observation of the Directional Wave Spectrum Evolution from Shoreline to Fully Developed, *J. Phys. Oceanogr.*, 19(5), 670–690, doi:10.1175/1520-0485(1989)019<0670:AOOTDW>2.0.CO;2, 1989.

Yan, L.: An improved wind input source term for third generation ocean wave modelling. Rep. No. 87–8, Royal Dutch Meteor. Inst. 20 pp, 1987.

605

Yang, Z., Neary, V. S., Wang, T., Gunawan, B., Dallman, A. R. and Wu, W.-C.: A wave model test bed study for wave energy resource characterization, *Renewable Energy*, 114(Part A), 132–144, doi:10.1016/j.renene.2016.12.057, 2017.

610

615



**Table1: Information on NDBC stations used for evaluation of model results**

Buoy	Depth(m)	Description	Longitude	Latitude
41004	38.4	EDISTO - 41 NM Southeast of Charleston, SC	-79.099	32.501
41048	5340	WEST BERMUDA - 240 NM West of Bermuda	-69.590	31.86
44011	82.9	GEORGES BANK 170 NM East of Hyannis, MA	-66.619	41.098
44017	52.4	MONTAUK POINT - 23 NM SSW of Montauk Point, NY	-72.048	40.694

620

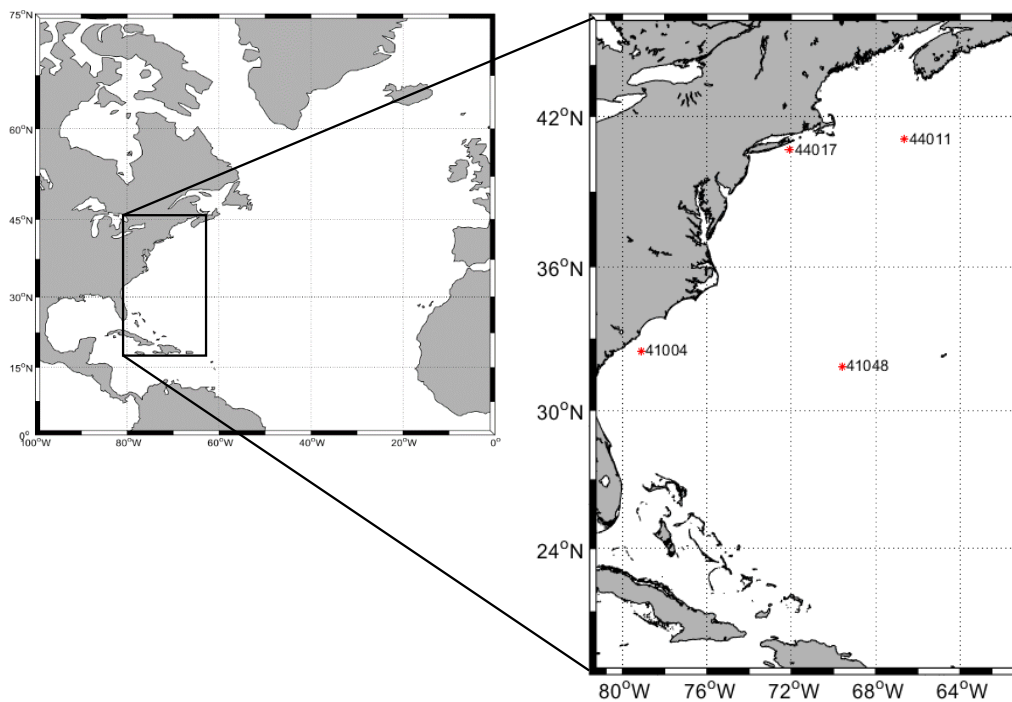
625

**Table 2: Simulated wave heights and mean periods using Komen and Westhuysen whitecapping methods at reference times t1 and t2 compared to observations at the four NDBC buoys.**

t1(01/08/2009 12:00)						
Buoy	Wave height(m)			Wave Period(sec)		
	Measurement	Komen	Westhuysen	Measurement	Komen	Westhuysen
41004	2.02	1.76	1.48	4.74	3.99	3.61
444017	5.05	3.53	3.17	7.19	5.78	4.89
41048	3.44	3.39	2.76	6.93	7.65	5.74
44011	6.20	6.04	5.57	7.71	8.25	6.83
t2 (01/21/2009 06:00)						
Buoy	Wave height(m)			Wave Period(sec)		
	Measurement	Komen	Westhuysen	Measurement	Komen	Westhuysen
41004	1.61	1.55	1.02	4.91	3.74	3.23
444017	1.87	1.56	1.49	4.52	3.99	3.84
41048	6.07	5.59	5.02	8.62	8.11	6.70
44011	2.26	2.21	1.94	5.52	5.01	4.58

630

635



640 **Figure 1: Modeling area and locations of NDBC buoys used for evaluation of whitecapping models**

645

650

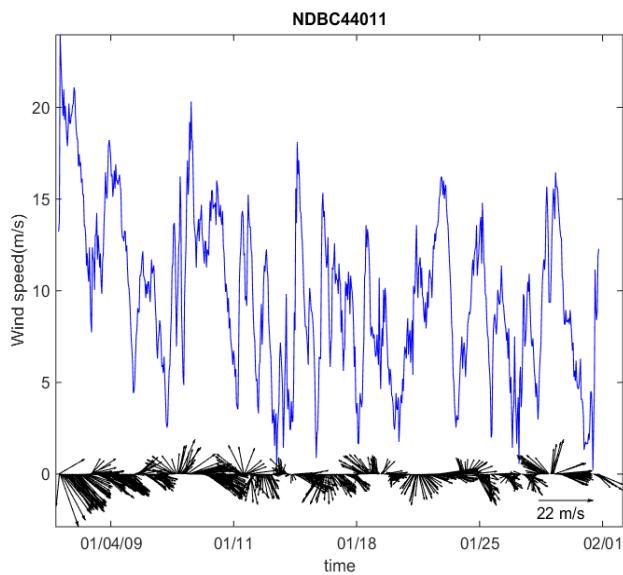
655

660



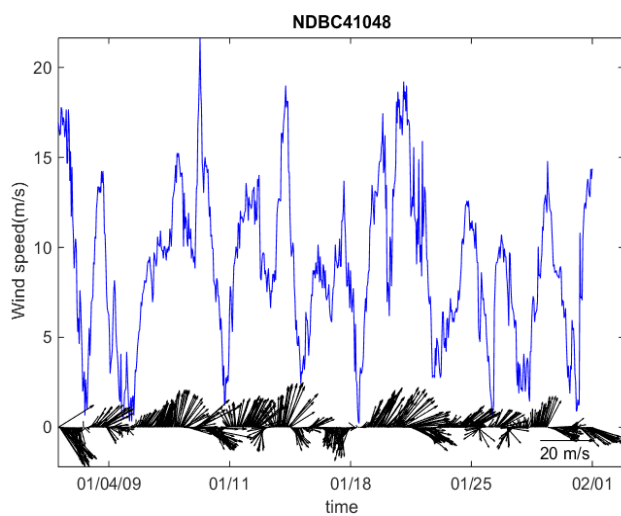
665

670



675

680

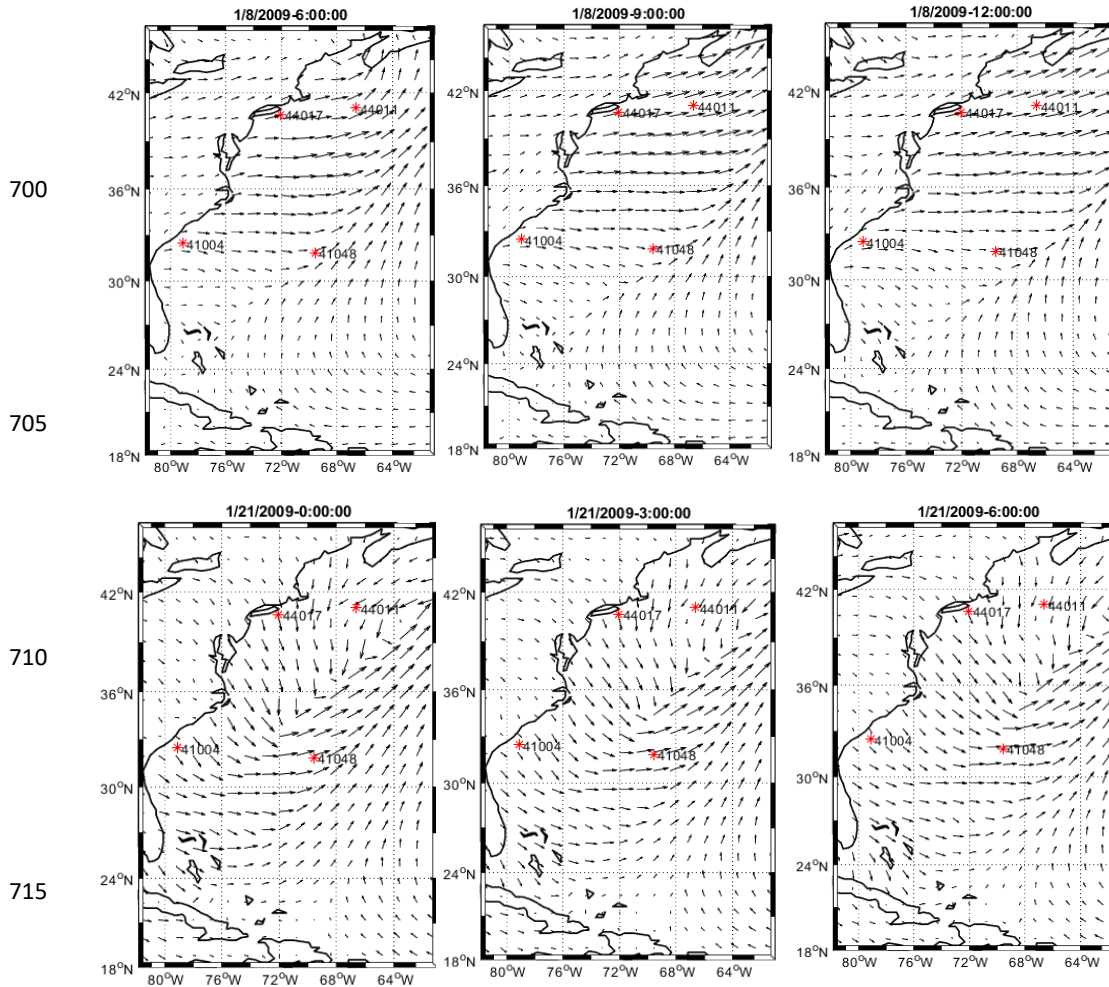


685

**Figure2: Time series of measured wind speed (lines) and vectors (arrows) at NDBC buoys 44011 (upper) and 41048 (lower).**

690

695



700

705

710

715

Figure 3: Three-hourly snapshots of CFSR wind fields over the modeling area ending at times t1 (1/8/2009 12:00, upper panels) and t2 (1/21/2009 06:00, lower panels).

720

725

730

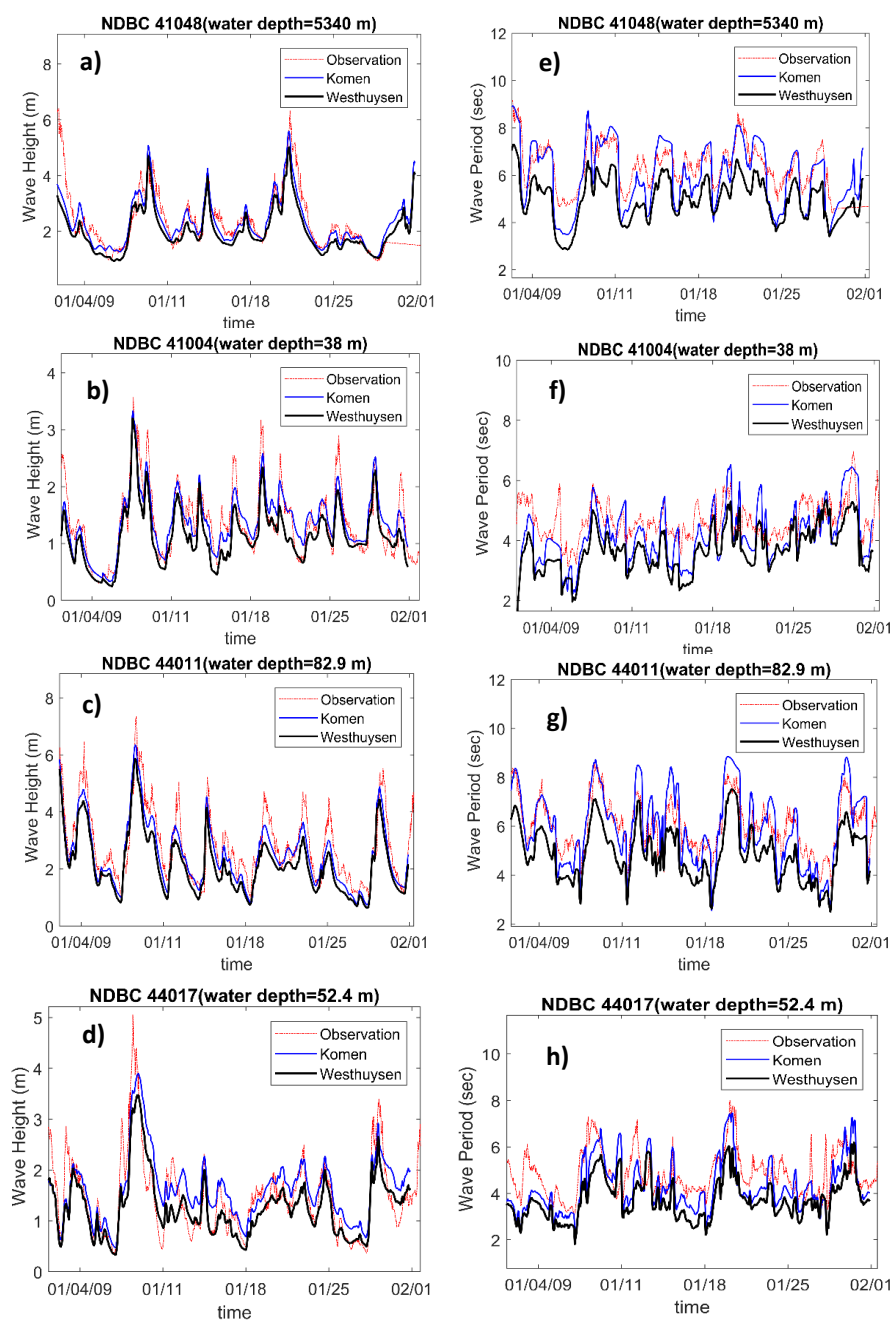
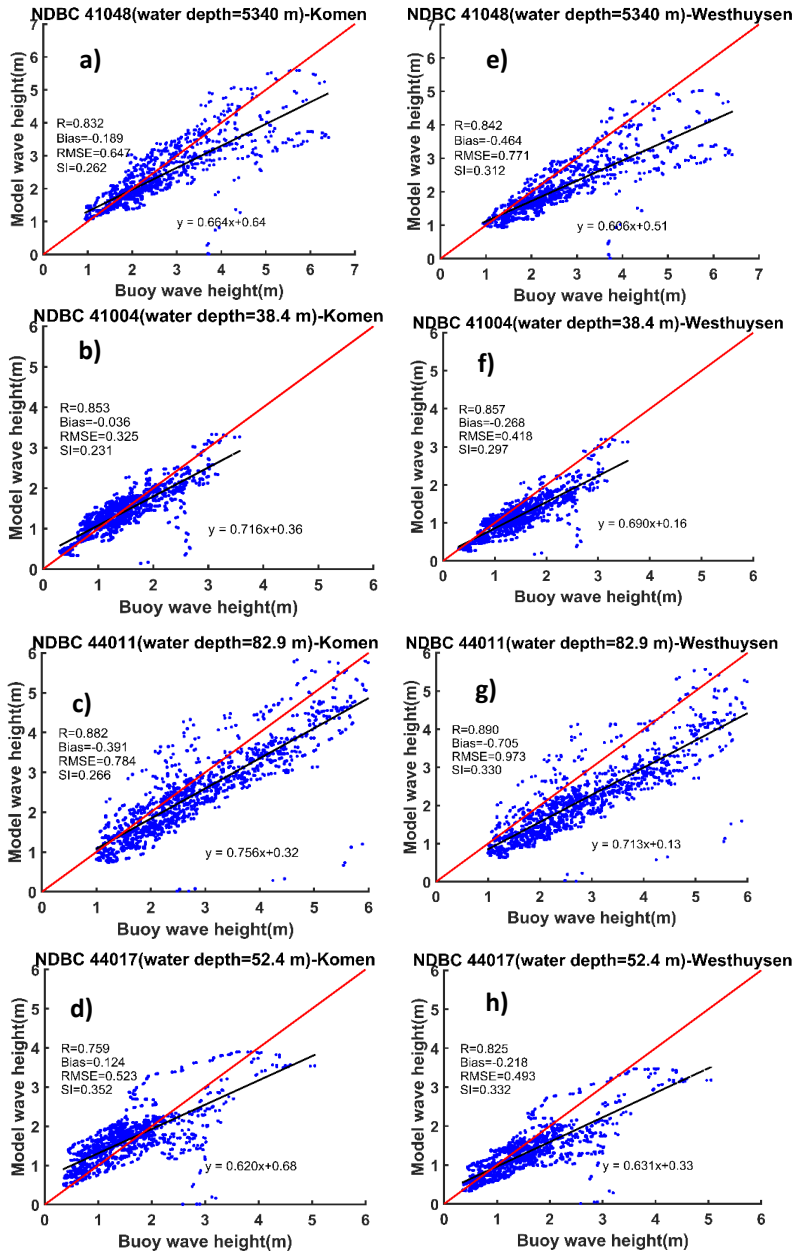


Figure 4: a-d) Time series of simulated wave heights and e-h) simulated mean wave periods, using Komen (blue lines) and Westhuysen (black lines) whitcapping formulas compared to measurements at the four NDBC buoys (dashed red lines).



735

Figure 5: Scatter plots and model performance metrics for simulated wave heights using a-d) Komen whitecapping, and e-h) Westhuysen whitecapping at the NDBC buoys.

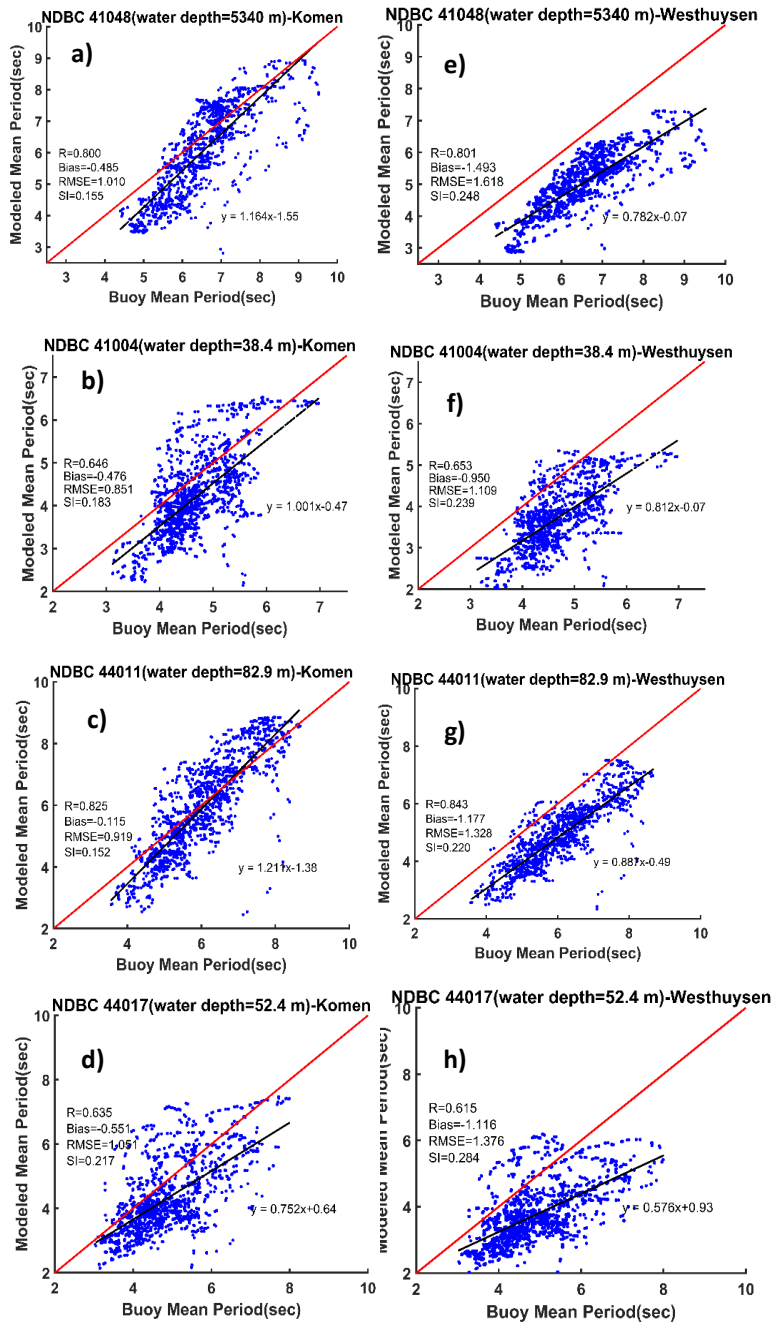
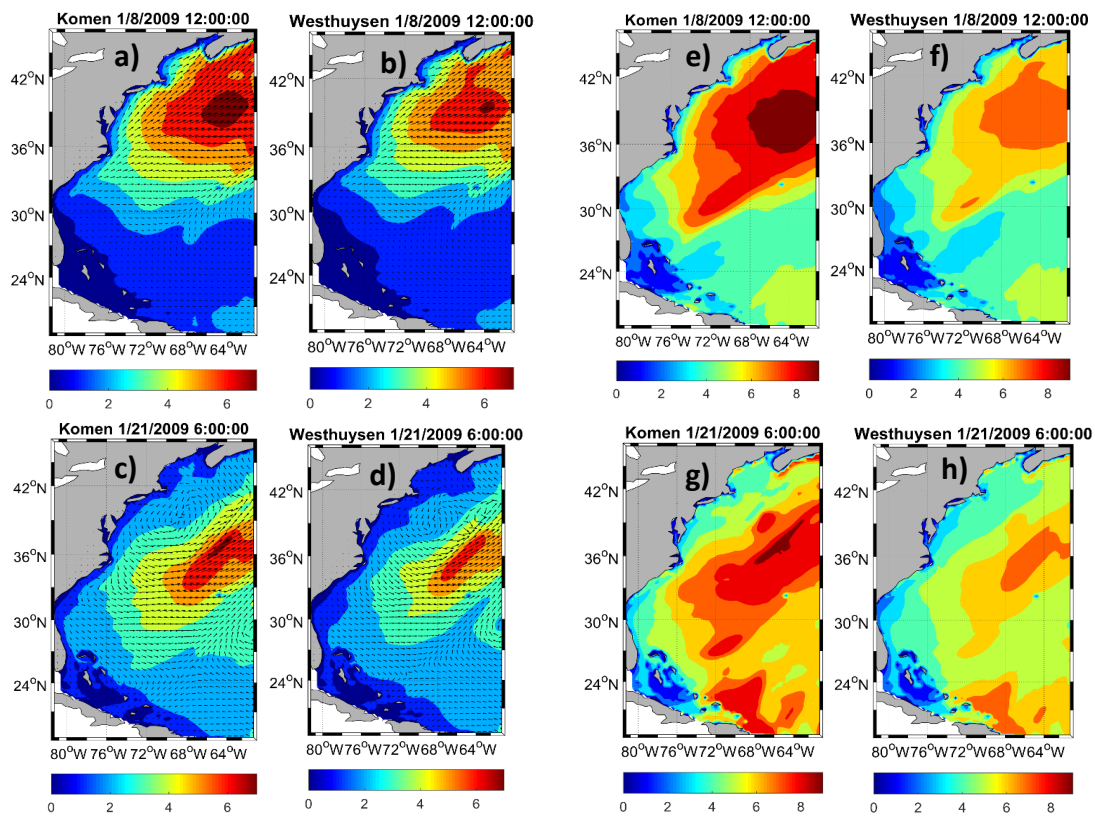


Figure 6: Scatter plots and model performance metrics for simulated mean wave period using a-d) Komen whitecapping, and e-h) Westhuysen whitecapping at the NDBC buoys.

740



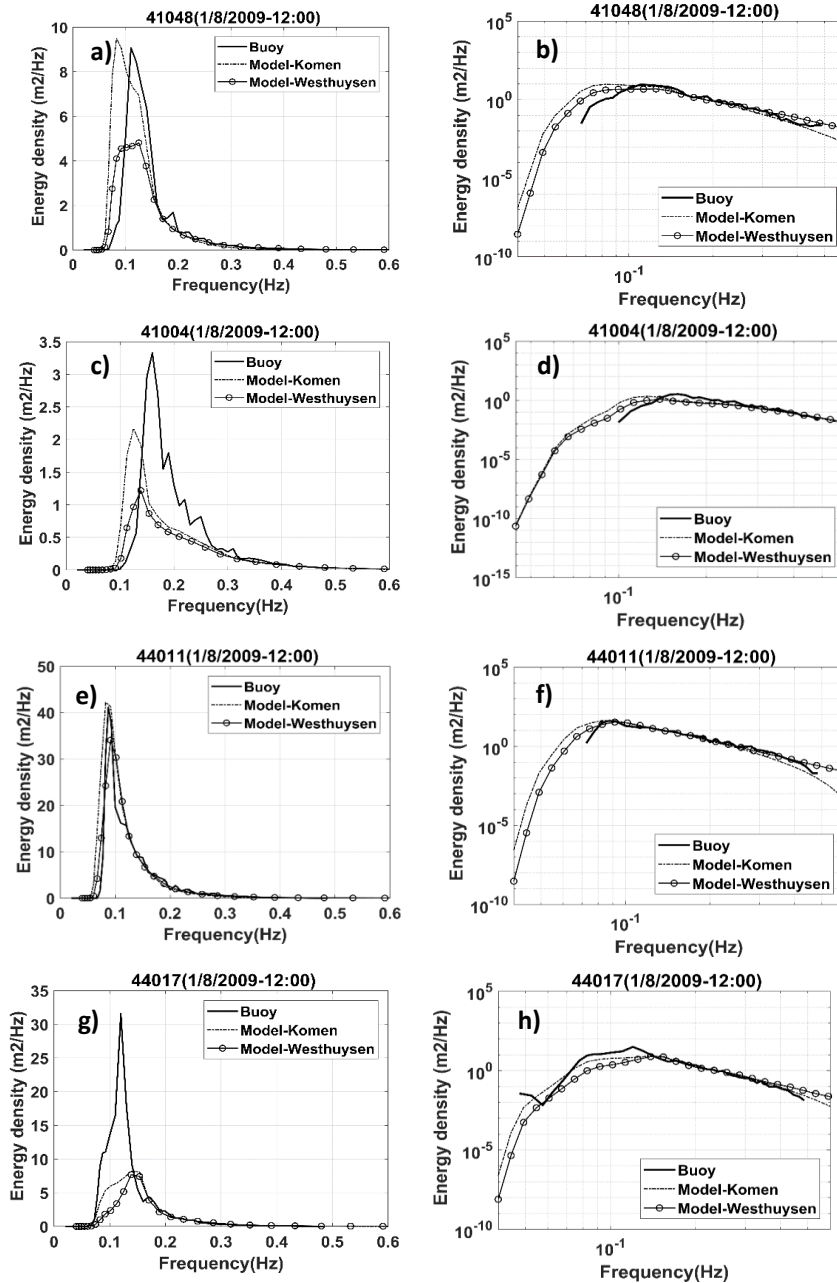
**Figure7:** a-d) Simulated wave height and direction over the modeling area using Komen and Westhuysen whitecapping formula for timesteps t1 (a and b) and t2 (c and d). e-h) Simulation results for mean wave periods for timesteps t1 (e and f) and t2 (g and h).

745

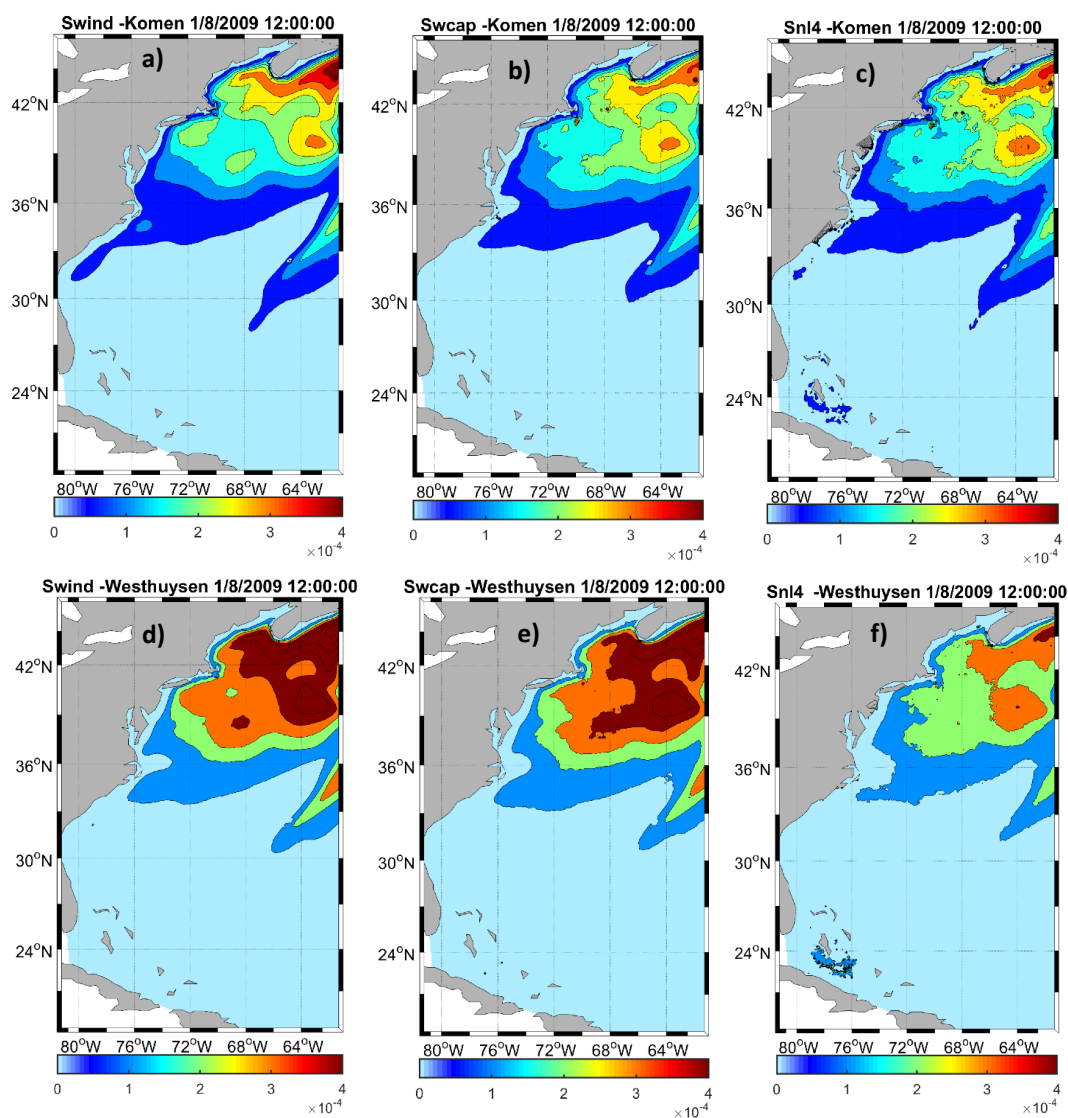
750

755

760



765 **Figure 8:** Comparison between the observed (solid lines) and simulated (dashed for Komen, circles for Westhuysen) frequency spectra at t1 at the four NDBC stations: a,c,e,g) linear scale for the energy axis and b,d,f,h) logarithmic scale for the energy axis.



770 **Figure 9:** Spatial variations of source terms (wind input, whitecapping dissipation, and quadruplet in  $w/m^2$ ) over the modeling area at time  $t_1$ , for a-c) Komen and d-f) Westhuysen.

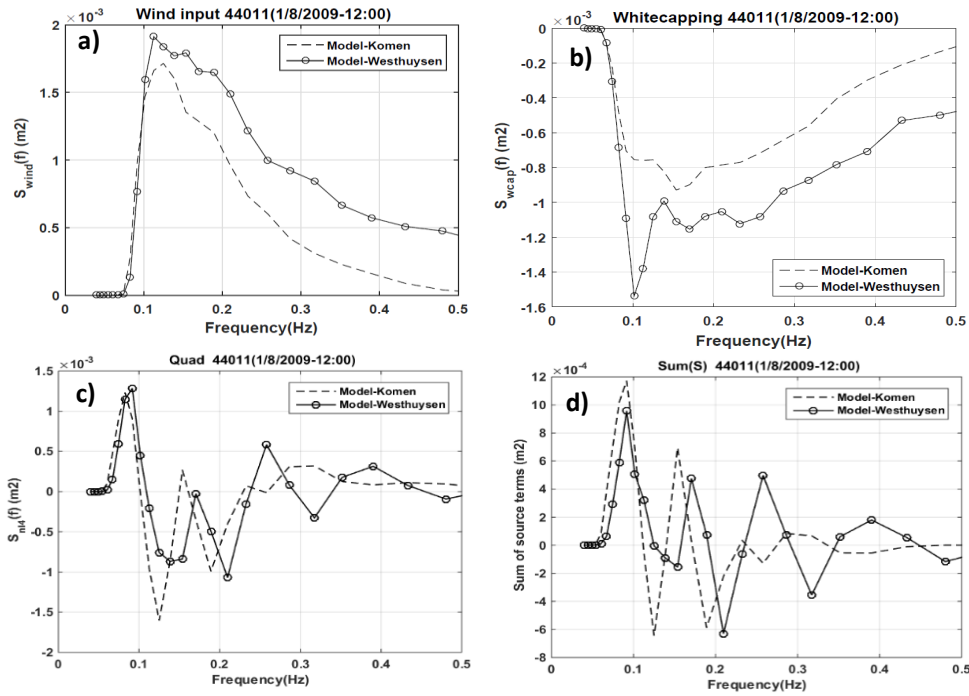


Figure 10: Variations of simulated source term components with frequency at buoy 44011 for t1: a) wind input, b) whitecapping dissipation, c) quadruplet, and d) algebraic sum of these terms.

780

785

790

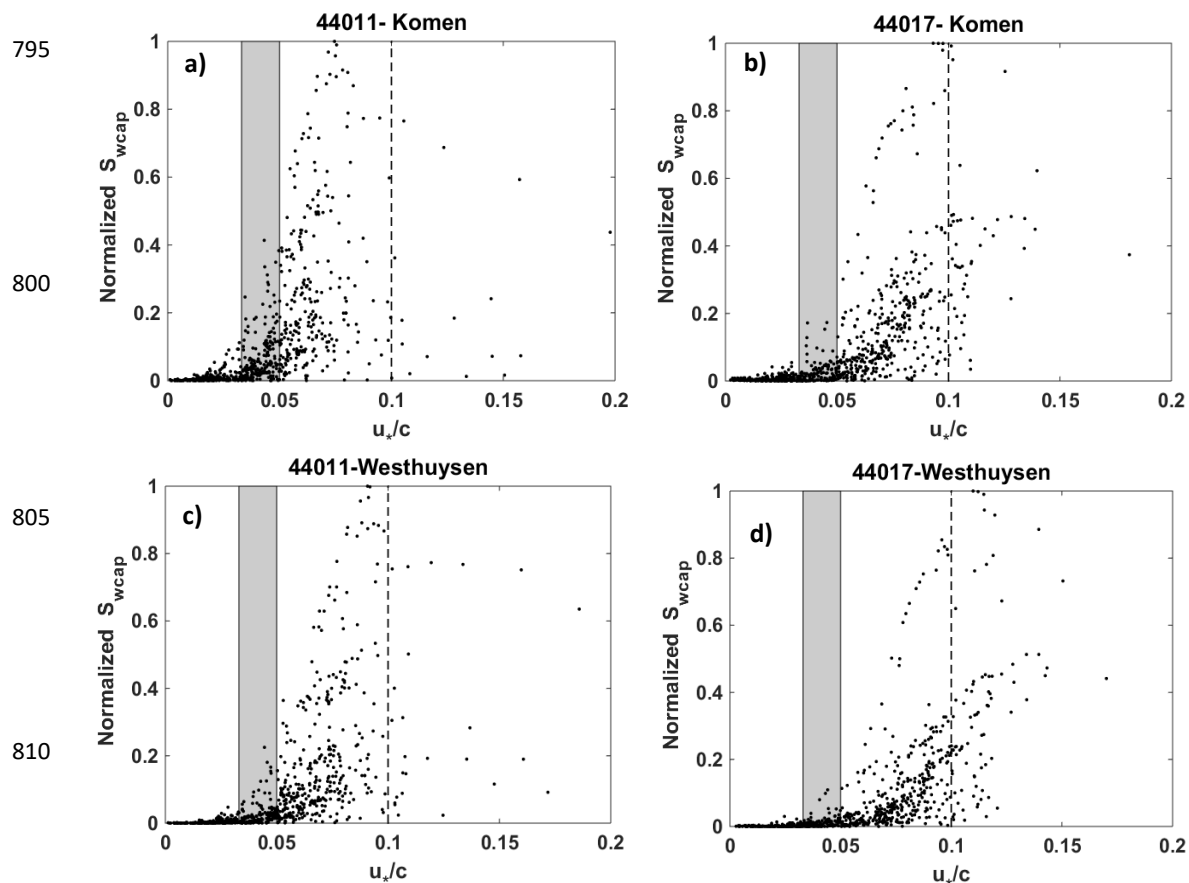


Figure 11: Variations of the normalized whitecapping dissipation ( $S_{wcap}$ ) from Komen and Westhuysen simulation scenarios with the inverse wave age  $\frac{u_w}{c}$  at a) and c) NDBC 44011, and b) and d) NDBC 44017. Gray boxes indicate the fully-developed zone ( $0.033 < \frac{u_w}{c} < 0.05$ ). The dashed line separates zones for linear and quadratic growth based on Yan(198y) as indicated by  $\frac{u_w}{c} = 0.1$ .

820

825

830

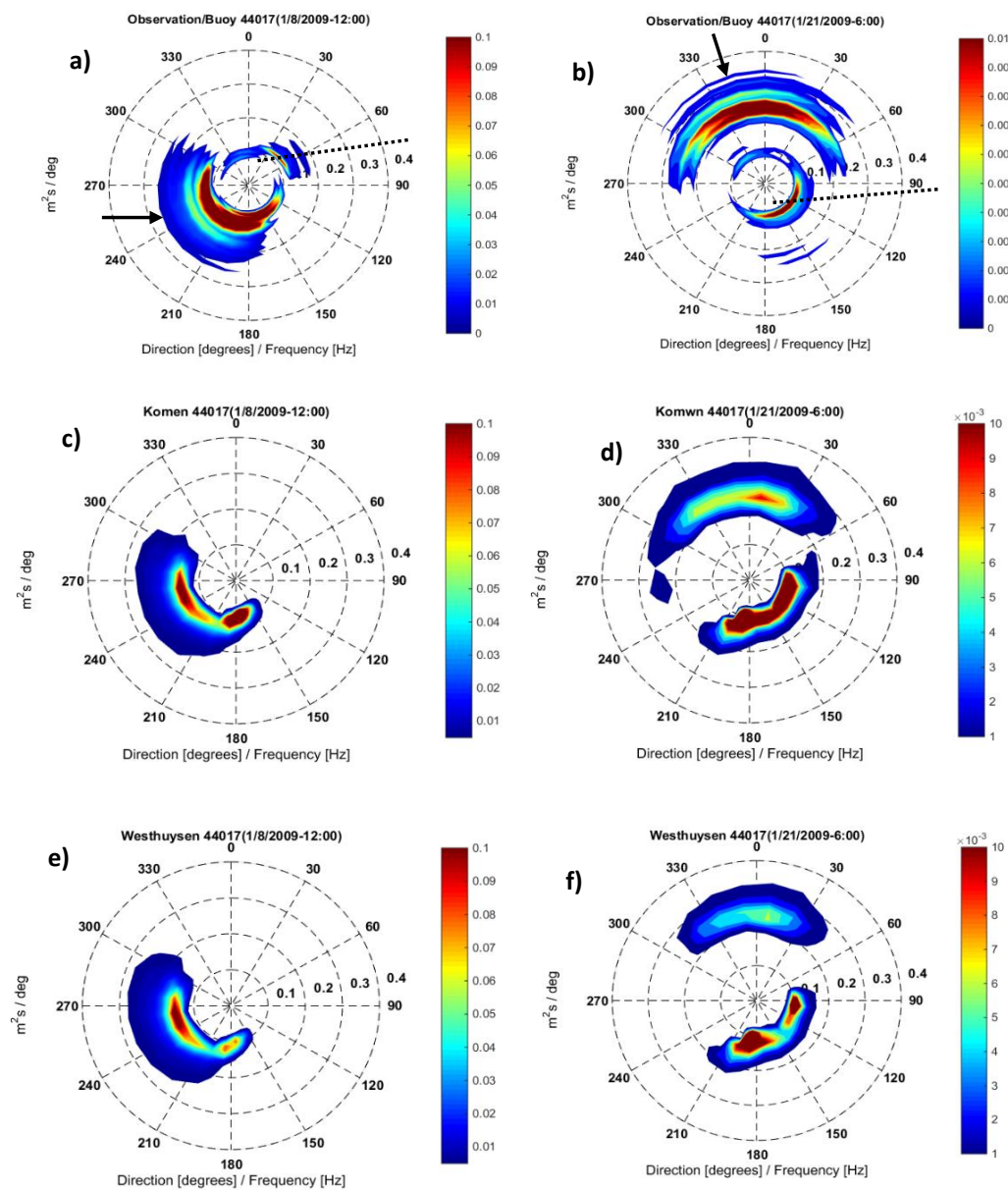
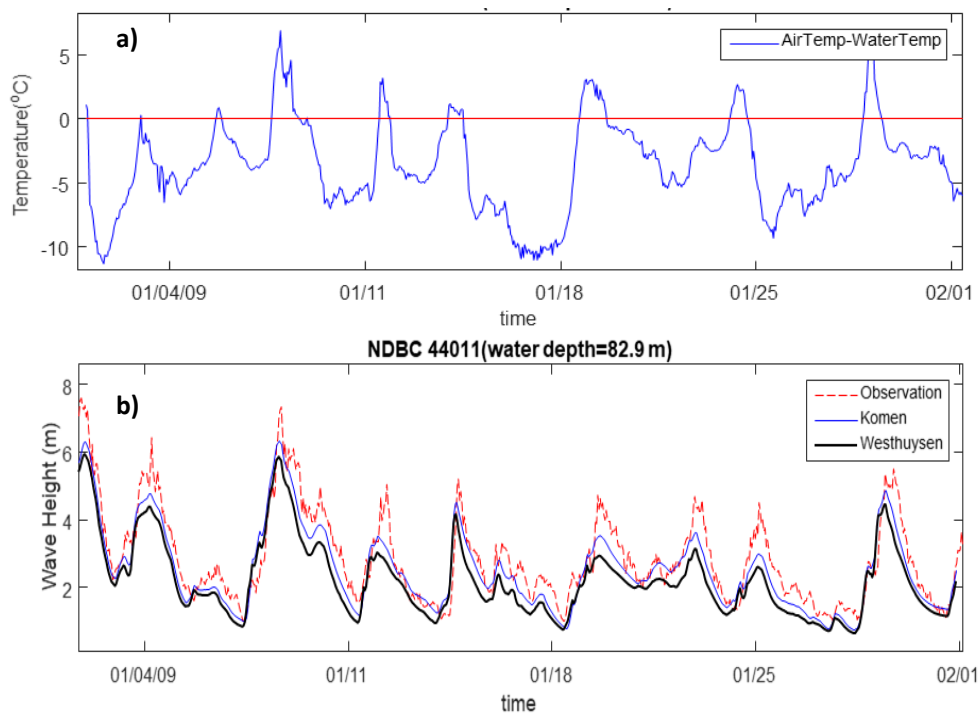


Figure 12: a,c,e) Frequency-directional spectra from observation, Komen simulation, and Westhuysen simulation, respectively at 44017 for time t1, b, d, f) the same spectra at t2. The solid arrows show the direction of observed CFSR wind at the buoy. The direction of the shoreline in the vicinity of the buoy is shown with dotted lines.



**Figure 13:** a) Time variations of the observed temperature difference between air and sea surface during January 2009 at buoy 41011. b) Time series of observed and simulated wave heights during this period.

840

845